Monthly Notices
of the Royal Astronomical Society

BC Gru: a spotted evolution shallow-contact binary in hierarchical triple system

Journal:	*Monthly Notices of the Royal Astronomical Society*
Manuscript ID	MN-23-4597-MJ
Manuscript type:	Main Journal
Date Submitted by the Author:	09-Nov-2023
Complete List of Authors:	Liao, wenping; Yunnan Observatories, Chinese Academy of Sciences, Qian, Shengbang; School of Physics and Astronomy, Yunnan University, Kunming 650091, China Li, Ping; Yunnan Observatories, Chinese Academy of Sciences, Kunming 650216, China Li, Linjia; Yunnan Observatories, Chinese Academy of Sciences, Kunming 650216, China Eduardo, Fernandez-Lajus; Facultad de Ciencias Astronomicas y Geofisicas, Universidad Nacional de La Plata, Paseo del Bosque S/N{B1900FWA, La Plata, Argentina; Instituto de Astrofisica de La Plata (CCT La Plata{CONICET/UNLP), B1900FWA La Plata, Argentina He, Jiajia; Chinese Academy of Sciences, Yunnan Observatories Liu, Nian-Ping; Yunnan Astronomical Observatory, Zeng, Qi-Huan Fang, Xiao-Hui
Keywords:	Stars, (stars:) binaries (including multiple): close < Stars, (stars:) binaries: spectroscopic < Stars, (stars:) binaries: eclipsing < Stars, stars: evolution < Stars, stars: individual:... < Stars

Mon. Not. R. Astron. Soc. **000**, 000–000 (0000) Printed 9 November 2023 (MN LATEX style file v2.2)

BC Gru: a spotted evolution shallow-contact binary in hierarchical triple system

WenPing Liao[1,2,3,4⋆], ShengBang Qian[5], Ping Li[1,4], LinJia Li[1,2,3], Fernández-Lajús Eduardo[6,7], JiaJia He[1,2,3], NianPing Liu[1,2,3], QiHuan Zeng[1,4], XiaoHui Fang[8]

[1] *Yunnan Observatories, Chinese Academy of Sciences, Kunming 650216, China*
[2] *Key Laboratory of the Structure and Evolution of Celestial Objects, Chinese Academy of Sciences, Kunming 650216, China*
[3] *Center for Astronomical Mega-Science, Chinese Academy of Sciences, 20A Datun Road, Chaoyang Dis- trict, Beijing, 100012, P. R. China*
[4] *University of Chinese Academy of Sciences, No.1 Yanqihu East Rd, Huairou District, Beijing, P.R.China 101408*
[5] *School of Physics and Astronomy, Yunnan University, Kunming 650091, China*
[6] *Facultad de Ciencias Astronómicas y Geofísicas, Universidad Nacional de La Plata, Paseo del Bosque S/N–B1900FWA, La Plata, Argentina*
[7] *Instituto de Astrofísica de La Plata (CCT La Plata–CONICET/UNLP), B1900FWA La Plata, Argentina*
[8] *School of Mathematics, Physics and Finance, Anhui Polytechnic University, Wuhu 241000, China*

ABSTRACT

BC Gru is a southern triple system that contains spectral types of approximately K0, K0, and K components. To understand the physical and orbital properties of this special system and the evolution state, we conduct a detailed joint study combining TESS and ground-based CASLEO observations. It is revised that BC Gru is an A-subtype shallow-contact binary with a mass ratio of 0.7. The discovery of variations in O'Connell effect could be explained by the evolution of cool and hot spots on the primary and secondary component, respectively. The $(O-C)$ curve constructed by 399 eclipse times shows a cyclical variation with a semi-amplitude of 0.016 days and a period of 58.37 yr. The cyclical change can be analyzed for the LTTE via the presence of third body that is orbiting around the central eclipsing binary in an eccentric orbit of $e_3 = 0.17$. It is suggested that the third body is probably a late K-type star. The orbital inclination is determined to be $i_3 \sim 30°$, which reveals that the third body is non-coplanar to the orbit of the central eclipsing binary. Further, we discovery that the variations of Max I and Max II coincide with the $(O-C)$ pattern of primary and secondary light minima during TESS observations, which indicates that the very low amplitude variability of ~ 0.0006 day found in the $(O-C)$ curve is most likely caused by star spots.

Key words: stars: binaries (including multiple) : close – stars: binaries : spectroscopic – stars: binaries : eclipsing — stars: evolution – stars: individual (BC Gru)

1 INTRODUCTION

In a recent joint study combining photometric and spectroscopic measurements, Liu et al. (2023) stated that the K-type contact binaries (CBs) have the shortest orbital periods among W UMa binaries, thus they are essential for the study of the A/W-subtype problem. They found that almost all of their early K-type CBs are W-subtype systems, except for a few samples that have nearly identical temperatures for binary components, and this special W-subtype phenomenon for K-type CBs should be further checked with more samples in the future. The formation and evolution of short period CBs is not well understood. In a series of research on "contact binaries with additional components" (Pribulla & Rucinski 2006; D'Angelo et al. 2006; Rucinski et al. 2007, papers I–III, respectively), the authors suggest that CBs may have formed in triple or larger multiple systems, where the tertiary companions may facilitate or enable the formation of CBs via acquiring and/or absorbing angular momentum during the evolution of multiple systems, especially if the tertiary components were in an eccentric orbit.

BC Gru ($V = 10.74$ mag) was discovered by Hoffmeister (1963) in his photographic search for variable stars in southern star fields. Later it was included in the catalog of 63rd Name-list of variable stars (S 6498 [4001], Kholopov et al. 1978). Its photographic light curve and several eclipse times were published by Meinunger (1979). She derived also an early period of 0.26617 day and concluded that BC Gru

⋆ E-mail: liaowp@ynao.ac.cn

is either a W UMa-type variable or an RRc-type variable. In the 4th Edition of General Catalogue of Variable Stars (GCVS) BC Gru is classified as EW:/KW: (Kholopov et al. 1985).

In the progress on the photometric study of short-period eclipsing binaries (Gomez et al. 1988), the V photoelectric partial light curve of BC Gru was obtained, showing a W UMa system with rather shallow eclipse, and an improved ephemeris was presented. The period of BC Gru was substantially modified to a longer value 0.3073070 ($\pm$0.0000098) day by them. Plewa & Kałużny (1992) revised the period to be 0.307356 ($\pm$0.000019) day from their multi-color photoelectric data. Their UVI light curves show only marginally asymmetric. The spectral type of G8V was suggested by them based on their color curves, and the primary component temperature was estimated to T_1 =5450 K. Simultaneous solutions of $BVRcIc$ light curves indicate that BC Gru is in a rather shallow-contact configuration ($f = 1.1\%$) and belongs to the W-subtype ($q = 1.77$) CBs. Samec & Becker (1993) reported precision multi-band light curves and four eclipse times, another improved ephemeris with a period of 0.30735687 (4) was given. Their very preliminary analysis showed that BC Gru is a very shallow-contact W-subtype binary with a difference temperature of $\Delta T \sim 400$ K and a large mass ratio of $q = 0.8$ (i.e., $1/q = 1.25$ for W-subtype). Thereafter, those photometric information of BC Gru has been listed in several catalogs or statistics study on W UMa stars (Pribulla et al. 2003; Avvakumova et al. 2013; Latković et al. 2021).

It was not until 2007 that the spectroscopic observations of BC Gru were developed by Dall et al. (2007) through the Variable Star One-shot Project (VSOP). The FEROS (Fibre-fed Extended Range Optical Spectrograph) spectrum confirmed the contact binary nature of BC Gru, meanwhile, revealed a third component. All three components have approximately the same spectral types of K0, K0, and K. They reported rotational velocities with large errors $(vsini)_a = 165 \pm 50$ km/s and $(vsini)_b = 142 \pm 50$ km/s for the binary, and $(vsini)_c = 6 \pm 3$ km/s for the tertiary component of the system. Ten years later, Moriarty (2016) published the first period analysis of BC Gru, the period was revised to 0.3073060(1) day. Moriarty commented that further time series observations are required to determine the effect of the third component in the system on the period of BC Gru. Moriarty's another aim was to develop a model solution based on detailed BVI_c asymmetry light curves obtained in 2014 and 2015 with a 356-mm Schmidt-Cassegrain telescope. He concluded that BC Gru is a W-subtype W UMa binary: $q_{ph} = 1.2$; $i = 69°$; $f = 8\%$; $l_{3B} = 9\%$, $l_{3V} = 12\%$, $l_{3I_c} = 19\%$, and the discovery that the $(O-C)$ diagram variation with a small modulations of 0.001 to 0.002 day in 2014 and 2015 is most likely caused by star spots. The third light contribution in I_c-band is the highest indicates that the third body should be a late K-type star.

Stellar atmospheric parameters of BC Gru can be accessed via the CDS VizieR service[1], where catalogs are mainly based on the RAVE DR6 that are cross-matched with relevant astrometric and photometric catalogs, and are complemented by orbital parameters and effective temperatures based on the infrared flux method (Shank et al. 2022; Steinmetz et al. 2020; Kunder et al. 2017; Kordopatis et al. 2013): $T_{eff} = 5050 \pm 120$ K, $\log g = 0.738$ cm/s^2, $[Fe/H] = -0.404 \pm 0.110$ dex.

As mentioned above, BC Gru has been observed by spectroscopy and photometry, a K-type third companion was revealed by the foregoing FEROS spectrum, a preliminary period analysis and photometric model solutions were reported, but a measurable light-travel-time effect (LTTE) in the orbital period changes and a modern light-curve solutions are lacking. We now have a good opportunity to further study the period changes and the evolution state of BC Gru by utilizing a longer time series of observations over several years, such as the 27-day continuous photometry data from the one of the most important ongoing all-sky projects Transiting Exoplanet Survey Satellite (TESS, Ricker et al. 2015) and the multi-band data observed at Complejo Astronomico El Leoncito (CASLEO, see Sec. 2). Simultaneously, the parallax of 5.2956 (8678) mas in Gaia EDR3 (Gaia Collaboration 2020) will make us calculate the distance of binary. It is hoped that this joint study of ground-based and space photometric observations can help us understand the physical and orbital properties of this special triple system, the evolution of star spots on a short time scale, as well as analyse the correlation between the O'Connell effect (O'Connell 1951) and the high frequency, low amplitude variability in the $(O-C)$ diagram, etc.

2 NEW CCD OBSERVATION AND ECLIPSE TIMES ACCUMULATION

For this study, new photometric observations covering B, V, R_c, and I_c filters were performed for BC Gru during 11 nights from 2018 August to 2023 September. Our photometric observations were performed using two different telescopes at Complejo Astronomico El Leoncito (CASLEO, in Argentina): CASLEO 2.15 m and CASLEO 0.6 m. The detailed description of the adopted observational strategy and data reduction can be found in Agarwal et al. (2019). The phased observations for each night are displayed in Fig. 1 with different colors. Based on a series of eclipse light curves (hereafter LCs), a parabolic fitting method was used to determine eclipse times in different bands that are nearly the same as those determined with the Kwee & van Woerden (1956) method. Totally, 19 new eclipse times were obtained and are listed in Table 1.

In addition, TESS space mission can achieve continuous LCs of BC Gru. We downloaded the TESS LCs data from the service of the Mikulski Archive for Space Telescopes (MAST)[2], there are two sectors, tess-s0001(from BJD 2458325 to 2458353, about 27 days, with an exposure time of 2 minutes) and tess-s0028 (from BJD 2459061 to 2459087, about 25 days, with an interval of about 10 minute cadence). Finally, 327 eclipse times were determined by using the method mentioned by Shi et al. (2021), which are tabulated in Table 1, they are published in the machine-readable format. The sector for 2 minutes cadence (shown

[1] https://vizier.cds.unistra.fr/viz-bin/VizieR-4

[2] https://mast.stsci.edu/portal/Mashup/Clients/Mast/Portal.html

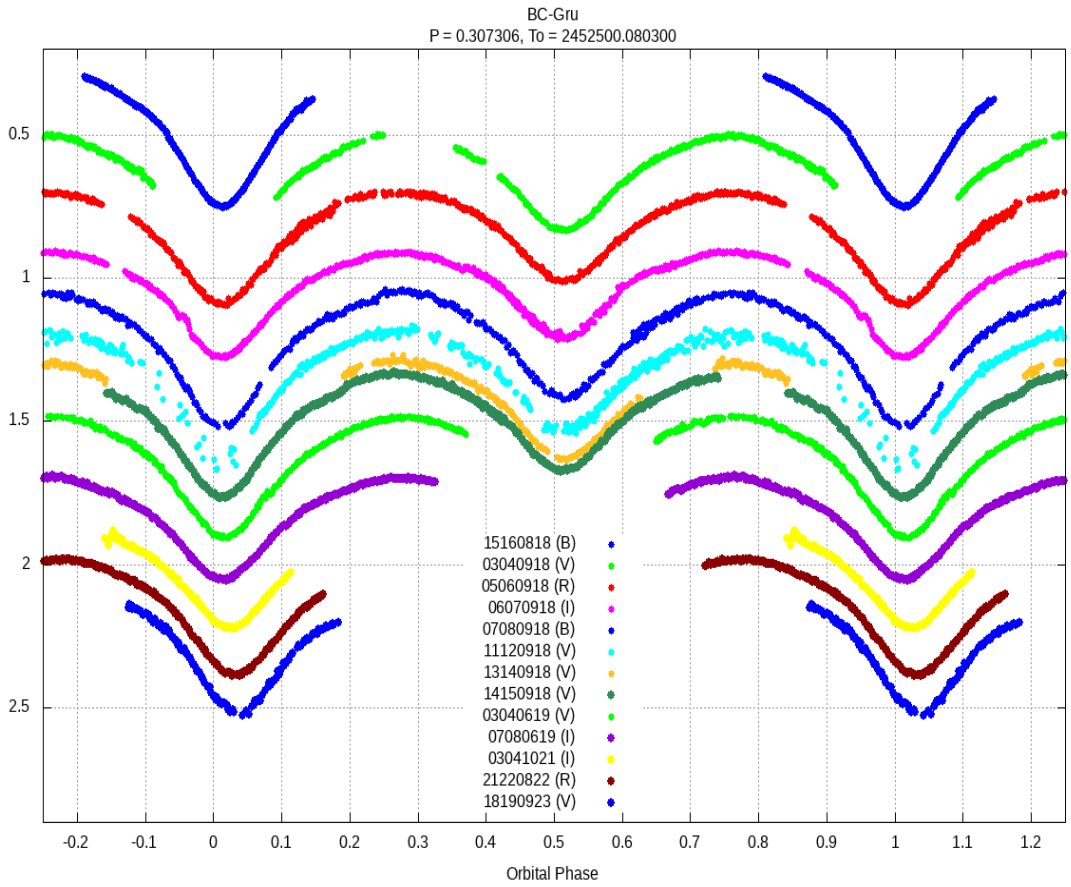

Figure 1. The phased eclipsing light curves observed at CASLEO, where different color lines represent different observational dates.

in the top of Fig. 2) together with the BVR_cI_c CASLEO LCs will be used to solve photometric model solutions and discuss the evolution of BC Gru system in Section 4. All the phased LCs after calculating with the equation of BJD = 2458325.37739 + 0.307306 × E are shown in the bottom of Fig. 2, where the color variation from dark blue to yellow represents changes over the time, and the Max I gets fainter and fainter, while the Max II has an opposite change.

3 PERIOD VARIATION ANALYSIS

Dall et al. (2007) reported that BC Gru is a triple system with same spectral types of about K0, K0, and K components. The rotational velocities for three components of the system were given with large errors by them. However, the physical and orbital characteristics of the third body have not been studied since then. Moriarty (2016) reported a simple continuous period increase pattern of BC Gru by using limited data points at that time, and revised the period of the binary system as 0.307306 day. As Moriarty (2016) pointed out, further time series of observations are required to determine the effect of the third body on period variations of the BC Gru, and to determine the influence of other causes of period changes. We totally collected 399 eclipse times for BC Gru, including 53 ones from literature, 327 new T-ESS eclipse times and 19 ones from CCD observations at CASLEO. All eclipse times are listed in the first Column of Table 1. Those shown in the Column 2 are errors of eclipse times, in the Columns 3-4 are eclipse types and sources of data, in the Column 7 are references of data. A detailed and improved analysis of period variations for the BC Gru system are given in this study. Expect to find a measurable LTTE in the orbital period analysis, and study the physical and orbital characteristics of the tertiary companion.

The epoch numbers and $(O-C)$ values were calculated with the following linear ephemeris, where T_0 is one of our new eclipse times,

$$MinI = 2458353.03435 + 0^{\rm d}.307306 \times E. \quad (1)$$

The epoch numbers and $(O-C)$ values are listed in the Columns 5-6 of Table 1 and plotted in the upper panel of Fig. 3. In the analysis of the $(O-C)$ diagram, an eccentric orbit of the tertiary component rotating around the central binary was considered. The trend of variations in $(O-C)$ curve was fitted with the following general equation (Irwin 1952),

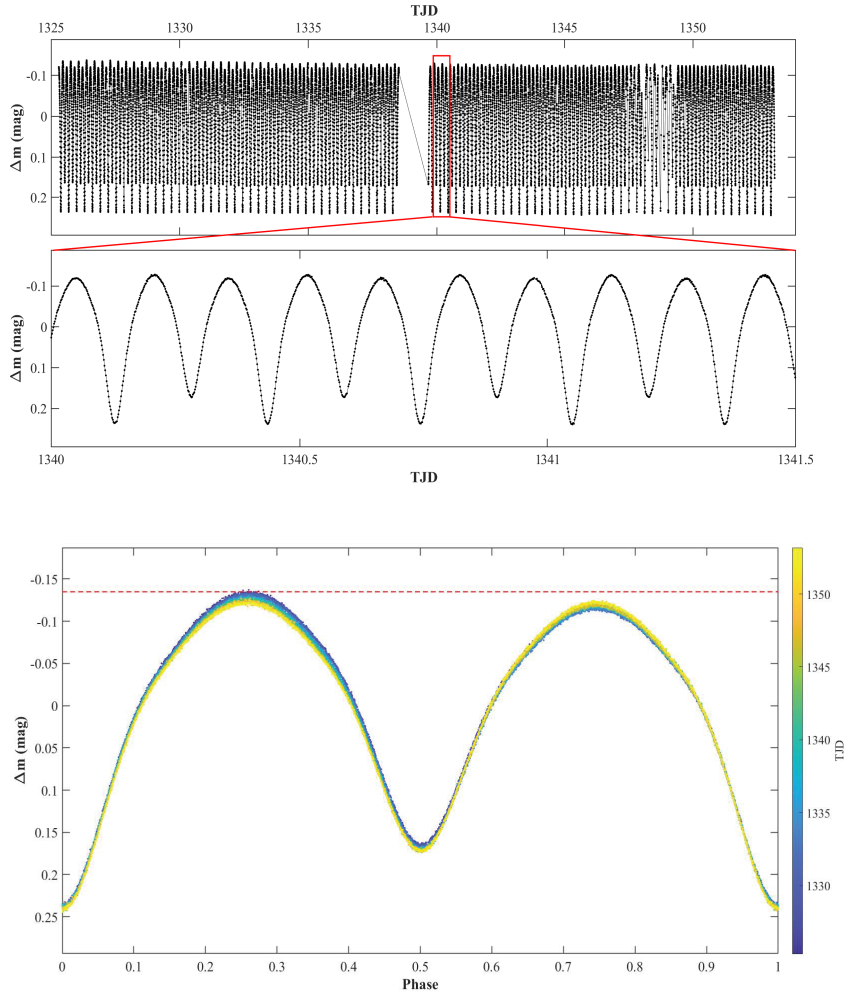

[hbp]

Figure 2. The TESS LCs of BC Gru with an interval of 2 minutes cadence (TJD = BJD-2457000.0), where the details of light curve for five cycles are also displayed in middle. Bottom panel: the phased TESS LCs, where the color variation from dark blue to yellow represents changes over the time.

$$
\begin{aligned}
O-C &= \Delta T_0 + \Delta P_0 E + \frac{\beta}{2}E^2 + A[(1-e_3^2)\frac{\sin(\nu+\omega)}{1+e_3\cos\nu} \\
&\quad + e\sin\omega] \\
&= \Delta T_0 + \Delta P_0 E + \frac{\beta}{2}E^2 \\
&\quad + A[\sqrt{1-e_3^2}\sin E^*\cos\omega + \cos E^*\sin\omega] \qquad (2)
\end{aligned}
$$

and the Kepler equation:

$$
M = E^* - e_3\sin E^* = \frac{2\pi}{P_3}(t-T_3), \qquad (3)
$$

where the meaning of each parameter is described in a recent paper of Liao et al. (2021).

Due to the low reliability of parabolic plus cyclical variation fitting, we tried to analyze the $(O-C)$ diagram without parabolic variation (i.e., $\beta = 0$). Its fitting results are shown in the upper panel of Fig. 3. The residuals of fitting are shown in the lower panel of Fig. 3. The $(O-C)_1$ diagram in the middle panel shows an apparent cyclic oscillation with a semi-amplitude of 0.016 day and a period of 58.37 yr. The corresponding fitted parameters are listed in Table 2.

In addition to the overall trend of changes mentioned above, we discover an obvious high frequency variability ($\sim$ 0.05 yr) with a very small modulation of 0.0006 day during TESS observations (shown in the top panel of Fig. 4), which is most likely caused by star spots (Kalimeris et al. 2002; Moriarty 2016). To study the correlation between the effect of star spots and such high frequency, low amplitude variability in the $(O-C)$ diagram during TESS observations, and to study the variation of LCs, the variations of the corresponding Max I and Max II from all the LCs are plotted in the middle and bottom panels of the Fig. 4. The middle panel shows the variations of Max I and Max II. The bottom panel presents the variations of the Max I - Max II, where the Max I - Max II between TJD 1325 - TJD 1345 are not close to zero, thus, we try to divide all of those asymmetrical LCs in this interval into three parts to analyse the spot evolution in Section 4: Part A (TJD 1325-1330), Part B (TJD 1333-1338) and Part C (TJD 1339-1344), separated by red and magenta dash lines. As one can see from Fig. 4, the variations of Max I and Max II coincide with the $(O-C)$ curves of the primary and secondary minima during TESS observations.

Table 1. A total of 399 times of light minima for BC Gru. This is a sample of the full table, which is available in its entirety in machine-readable format.

Eclipse Times HJD-2400000	Error (± days)	Eclipse P/S	Source	Epoch	$O-C$ (days)	References
36814.292		P	Literature	-70089	0.0279	(1)
46686.65316	0.00007	S	Literature	-37963.5	0.0301	(2)
46686.80628	0.00027	P	Literature	-37963	0.0296	(2)
46687.72825	0.00019	P	Literature	-37960	0.0297	(2)
46688.80488	0.00019	S	Literature	-37956.5	0.0307	(2)
.....	.....	.....	.....	.....	.....	.....
58345.96621	0.00008	P	TESS	-23	-0.0001	(8)
58346.12009	0.00011	S	TESS	-22.5	0.0001	(8)
58346.27354	0.00010	P	TESS	-22	-0.0001	(8)
58346.42734	0.00010	S	TESS	-21.5	0.0001	(8)
58346.58081	0.00007	P	TESS	-21	-0.0001	(8)
58346.73459	0.00013	S	TESS	-20.5	0.0000	(8)
58346.88811	0.00008	P	TESS	-20	-0.0001	(8)
58346.88813	0.00003	P	CASLEO 2.15m	-20	-0.0001	(8)
58347.04186	0.00011	S	TESS	-19.5	0.0000	(8)
58347.19530	0.00009	P	TESS	-19	-0.0002	(8)
58347.35037	0.00070	S	TESS	-18.5	0.0012	(8)
58347.50263	0.00008	P	TESS	-18	-0.0002	(8)
.....	.....	.....	.....	.....	.....	.....
58365.78787	0.00007	S	CASLEO 0.6m	41.5	0.0003	(8)
58367.63189	0.00010	S	CASLEO 0.6m	47.5	0.0005	(8)
58367.78495	0.00008	P	CASLEO 0.6m	48	-0.0001	(8)
58368.55314	0.00015	S	CASLEO 0.6m	50.5	-0.0002	(8)
58368.70674	0.00008	P	CASLEO 0.6m	51	-0.0002	(8)
58368.86090	0.00021	S	CASLEO 0.6m	51.5	0.0003	(8)
58369.62887	0.00008	P	CASLEO 0.6m	54	0.0000	(8)
58369.78319	0.00014	S	CASLEO 0.6m	54.5	0.0007	(8)
58373.62315	0.00045	P	CASLEO 0.6m	67	-0.0007	(8)
58373.77863	0.00020	S	CASLEO 0.6m	67.5	0.0011	(8)
58375.62187	0.00009	S	CASLEO 0.6m	73.5	0.0005	(8)
58376.54342	0.00008	S	CASLEO 0.6m	76.5	0.0002	(8)
58376.69716	0.00005	P	CASLEO 0.6m	77	0.0002	(8)
58638.82994	0.00007	P	CASLEO 0.6m	930	0.0010	(8)
58642.82426	0.00007	P	CASLEO 0.6m	943	0.0004	(8)
.....	.....	.....	.....	.....	.....	.....
59085.80779	0.00052	S	TESS	2384.5	0.0023	(8)
59085.96023	0.00077	P	TESS	2385	0.0011	(8)
59086.11482	0.00043	S	TESS	2385.5	0.0020	(8)
59086.26837	0.00084	P	TESS	2386	0.0019	(8)
59086.42194	0.00049	S	TESS	2386.5	0.0018	(8)
59086.57526	0.00062	P	TESS	2387	0.0015	(8)
59086.72977	0.00055	S	TESS	2387.5	0.0023	(8)
59086.88274	0.00083	P	TESS	2388	0.0017	(8)
59491.60682	0.00007	P	CASLEO 0.6m	3705	0.0037	(8)
59813.66589	0.00006	P	CASLEO 0.6m	4753	0.0061	(8)
60206.71151	0.00012	P	CASLEO 0.6m	6032	0.0074	(8)

References: (1)Paschke, A. (2010); (2) Plewa & Kaluzny (1992); (3) Gomez et al. (1988); (4) Samec & Becker (1993); (5) Pribulla et al. (2003); (6) Moriarty (2016); (7) Juryšek et al. (2017); (8) This paper.

4 MODERN LIGHT-CURVE SOLUTIONS

As shown in the middle panel of Fig. 4, the Max I and Max II between TJD 1349 and TJD 1353 are almost close, suggesting that the TESS LCs are symmetrical. Thus, the average LC of this time interval is selected to solve a model solution without spot. In addition, we also selected a set of symmetric CASLEO BVR_cI_c LCs (20180907B; 20180913, 14V; 20180905R_c; 20180906I_c) from the Fig. 1 to solve light-curve solution without spot. Except for the symmetrical LCs of TJD 1349 to TJD 1353, the TESS LCs of BC Gru are always asymmetric during $\sim$ 24 day continuous observations, exhibit a noticeable positive O'Connell effect, where the first light maximum at phase 0.25 (Max I) is brighter than the second maximum at phase 0.75 (Max II). It is a common and complex phenomenon in eclipsing binaries that Max I and Max II are not equal in height. Any mode that can cause local brightness change of the surface of the binary components, such as spots, mass transfer and so on, could cause this phenomenon (Shi et al. 2021; Liao et al. 2022). We divided these asymmetric TESS LCs into three segments, i.e., TJD 1325-1330, TJD 1333-1338, and TJD 1339-1344, which could provide a good opportunity to study the star spot's continuous evolution on short-time scales.

All LCs are analyzed by using 2015 Wilson–Devinney (W–D) code (Van Hamme & Wilson 2007; Wilson 2012 and Wilson & Devinney 1971). According to the spectral type K0 for the primary star (Star 1), its temperature is fixed to be 5240 K (Cox 2000), thus its gravity-darkening and bolometric albedos coefficients are set to $g_{1,2} = 0.32$ and $A_{1,2} = 0.5$. The bolometric and bandpass limb-darkening coefficients were obtained by using an internal computation with the logarithmic law.

To check the mass ratio values and sub-type of BC Gru, a series of trial values of q were assumed , i.e., a common technique called q-search method. The resulting mean residuals $\overline{\Sigma}$ for each q are plotted in left panels of Figs. 5-6 (Fig. 5 for TESS, Fig. 6 for CASLEO). As seen from these two left panels, the minimum values of $\overline{\Sigma}$ are achieved at $q = 0.65$

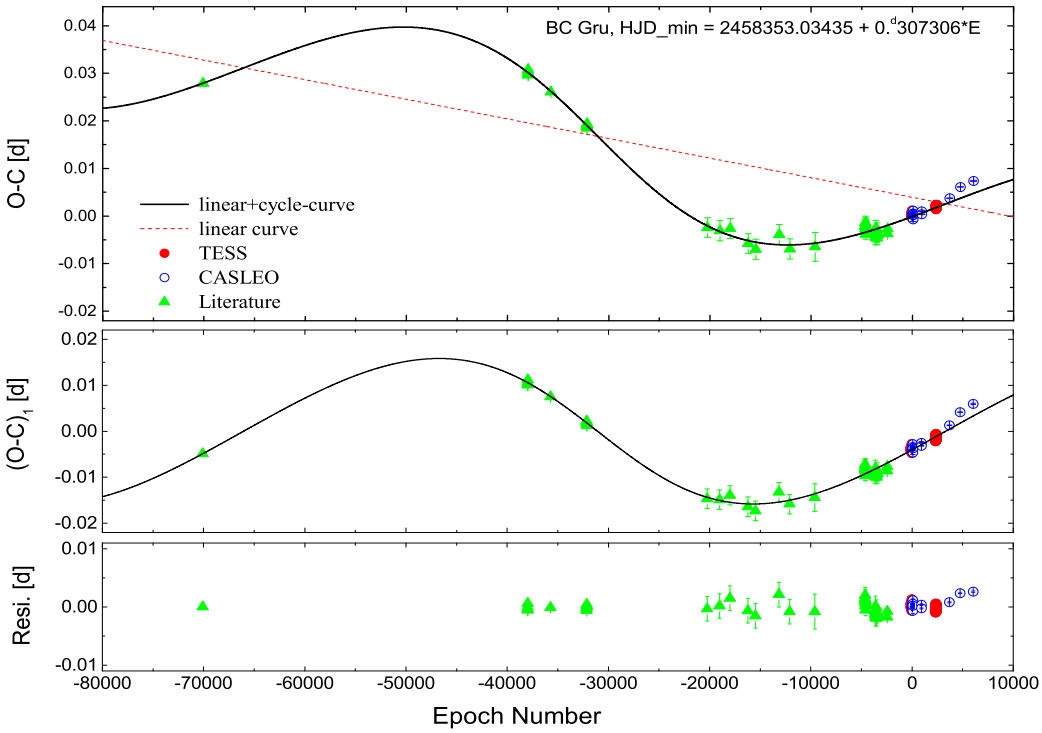

Figure 3. The $(O-C)$ diagrams of BC Gru fitted with an eccentric orbit for the pattern of linear plus cyclical fit. The data sources and colored lines are noted in the upper panel, the cyclical variations alone are shown in the middle panel, and the residuals from the whole effect are displayed in the bottom panel.

Table 2. Orbital parameters of the third body in the BC Gru system.

Parameters	Linear + cyclical variation
Revised epoch, ΔT_0 (days)	0.0039(±0.0035)
Revised period, ΔP_0 (days)	$-4.12(\pm1.21)\times10^{-7}$
Semi-amplitude, A (days)	0.0160 (±0.0019)
Orbital period, P_3 (yrs)	58.37 (±6.04)
Rate of the period change, $\dot{P}$ (day yr^{-1})	0 (assumed)
Longitude of the periastron passage, ω (deg)	184.46 (±9.60)
Time of periastron passage, T_3 (HJD)	2449025.03 (±0.06)
Eccentricity, e_3	0.17 (±0.08)
Projected semi-major axis, $a_{12}\sin i_3$ (au)	2.77 (±0.33)
Mass function, $f(m)$ ($M_\odot$)	0.0063 (±0.0022)
Mass, M_{3min} ($M_\odot$)	0.27 (±0.04)
Orbital semi-major axis, a_{3max} (au)	15.43 (±2.74)
The case of late K9-type tertiary companion:	
Mass, M_3 ($M_\odot$)	0.59 (assumed)
Orbital inclination, i_3 (deg)	30
Orbital semi-major axis, a_3 (au)	13.74 (±2.60)
Projected semi-major axis, a_{12} (au)	5.54 (±0.66)

and $q = 0.66$, respectively. Because the fact that the K-type tertiary in the system could contribute light to the total system, we decided to calculate a photometric solution with a third light. Therefore, in the process of fitting, we expanded the free parameters beyond just the mass ratio q, including the orbital inclination i; the effective surface temperature of secondary T_2; the monochromatic luminosity of primary L_1; the modified dimensionless surface potential ($\Omega_1 = \Omega_2$ for contact configuration Model 3); and the third light l_3. Iterations were performed with the initial input parameters of

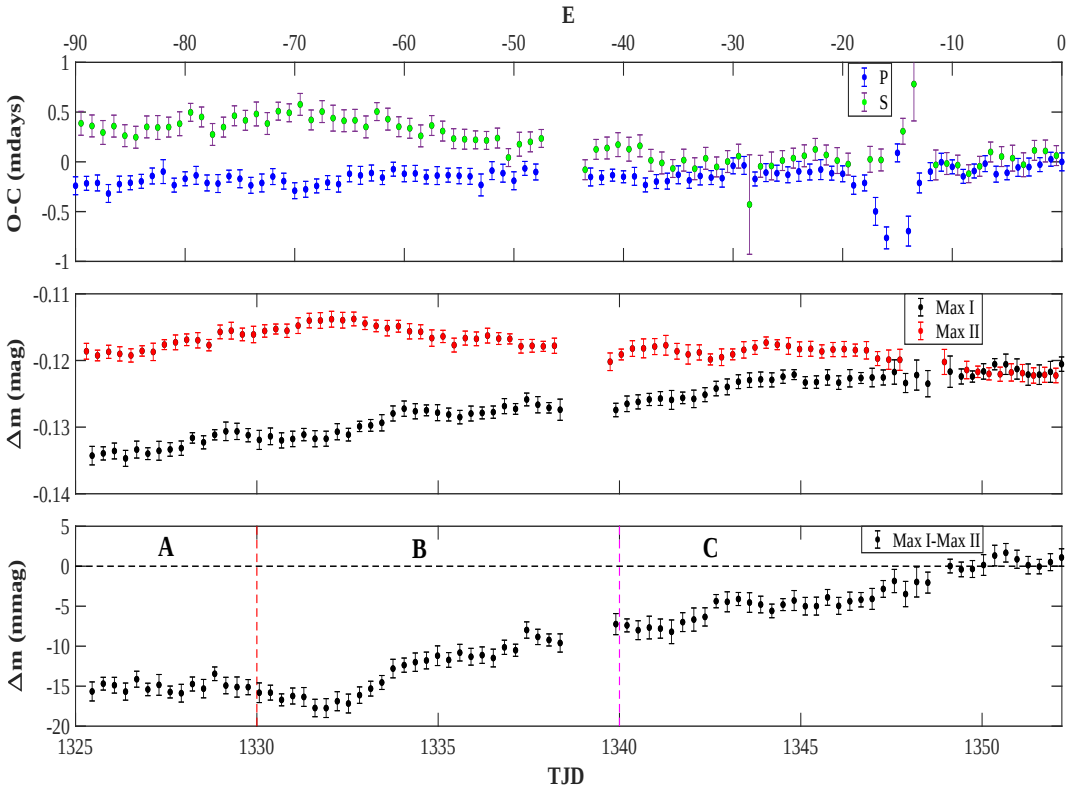

Figure 4. The variation trends of the $(O-C)$ curves during TESS observation, the Max I, the Max II, and the Max I - Max II. Top panel: the variations of the $(O-C)$ curves during TESS observation. Middle panel: the variations of the Max I and the Max II. Bottom panel: the variations of the Max I - Max II, where the variations during TJD 1325 - TJD 1345 can be divided into three parts A, B and C separated by red and magenta dash lines.

$q = 0.65$ and $q = 0.66$ until convergence. The final solutions with the third light l_3 were derived and listed in Columns 2 and 3 of Table 3 for symmetrical CASLEO and TESS LCs, respectively. The diagrams of without-spot fitting for TESS and CASLEO are shown in the right panels of Fig. 5 and Fig. 6, respectively. The observational LCs (the black circles), the theoretical fitting LCs (the solid colored lines), and the theoretical geometrical structure are displayed.

For the three asymmetric TESS LCs, we expanded the spot parameters as adjustable parameters (see note in Fig. 7 for details) beyond above free parameters. The final spots + third light solutions for three sets of asymmetric TESS LCs were derived and listed in the Columns 4-6 of Table 3, mean values of these three spotted solutions are shown in the Column 7. As one can see from the Table 3, the solutions of TESS LCs show much smaller mean residual values compared with that of CASLEO. Moreover, considering the fact of the asymmetric LCs during $\sim$ 24 day continuous observations and the existence of the third body, we will take the mean values of "spots & l_3" solutions for the following calculations and discussions.

The theoretical LCs described with a cool spot on the primary component and a hot spot on the secondary component plus a third light were displayed as red solid lines in the Fig. 7, in which the spots parameters and the theoretical geometrical structure for TESS are also shown. The two spots are roughly symmetrical with the inner Lagrange L1 point.

5 DISCUSSIONS AND CONCLUSIONS

BC Gru is a southern triple system that contains spectral types of about K0, K0, and K components. It has been observed by spectroscopy and photometry by several authors, a preliminary period analysis and photometric model solutions were reported, but a measurable LTTE in the orbital period changes and a modern light-curve solutions are required. By using a longer time series of observations over several years, i.e., the continuous photometry data from TESS and the multi-band data observed at CASLEO, a joint photometric study of space and ground-based observations for this special triple system was given in present paper.

The orbital period variations are re-analyzed in detail by using a total of 399 eclipse times. It is discovered that the $(O-C)$ curve of BC Gru shows a pattern of "linear + cyclical variation" with a semi-amplitude of 0.0160 ($\pm$0.0019) days and a period of 58.37 ($\pm$6.04) yr. The cyclical change in the $(O-C)$ diagram can be analyzed for the LTTE via the potential of a third body in an eccentric orbit. In addition to the overall trend of changes mentioned above, we also found an obvious high frequency variability ($\sim$ 0.05 yr) with a very small modulation of 0.0006 day during TESS observations.

According to the Table 5 of Pecaut & Mamajek (2013) and K0-type for primary component, its mass was set as $M_1 = 0.88$ M$_\odot$, the mass of secondary component was then calculated to be $M_2 = 0.62$ M$_\odot$ ($q_{ph} = 0.71$). Using the commonly used mass function equation of multi-

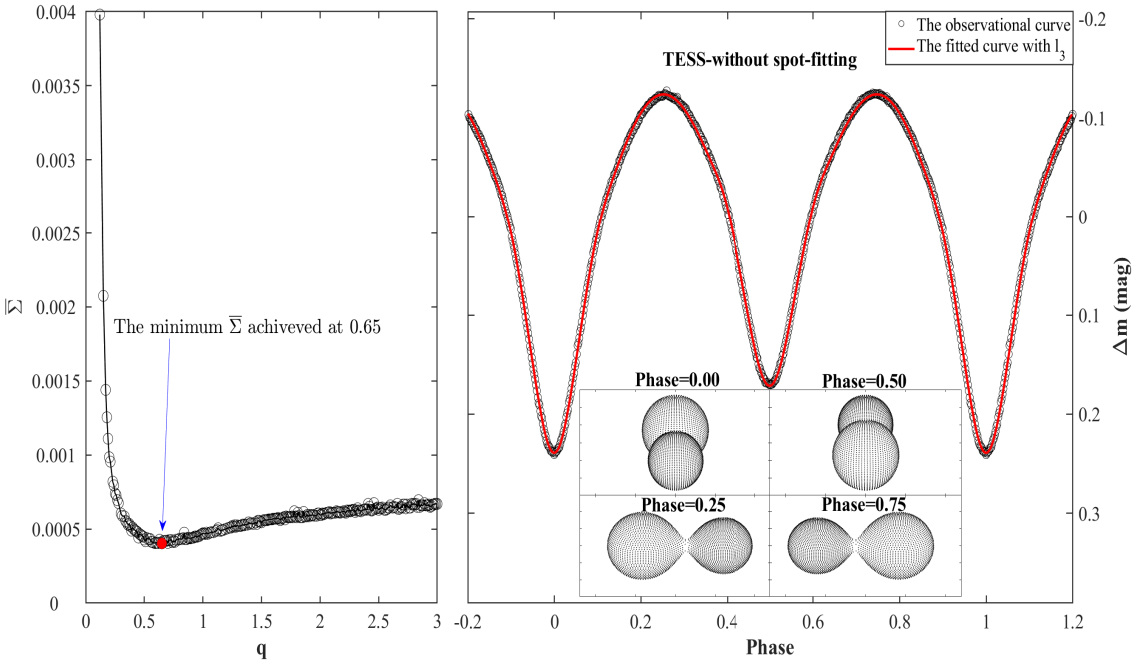

Figure 5. The diagram of without-spot fitting obtained using the W-D program. Left panel: the relation between q and $\overline{\Sigma}$ determined by model 3 for TESS. Right panel: the observation light curves (the black circles), the theoretical fitting light curves with the third light l_3 (the red solid line), and the theoretical geometrical structure for TESS.

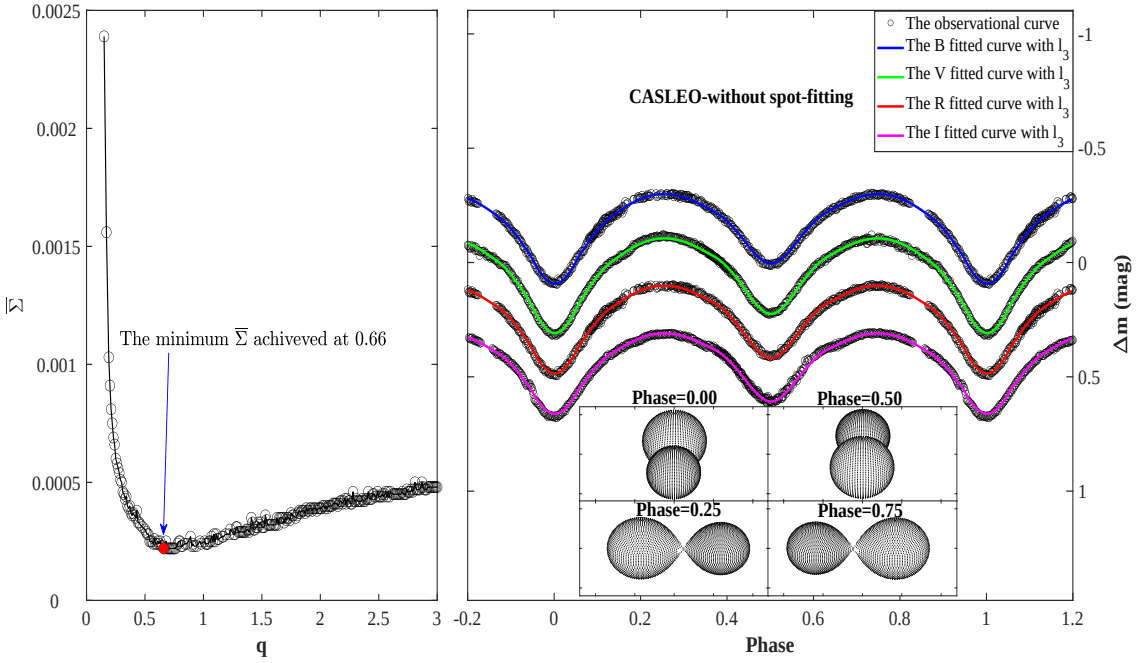

Figure 6. Same as the Fig. 5, but for CASLEO LCs fitting.

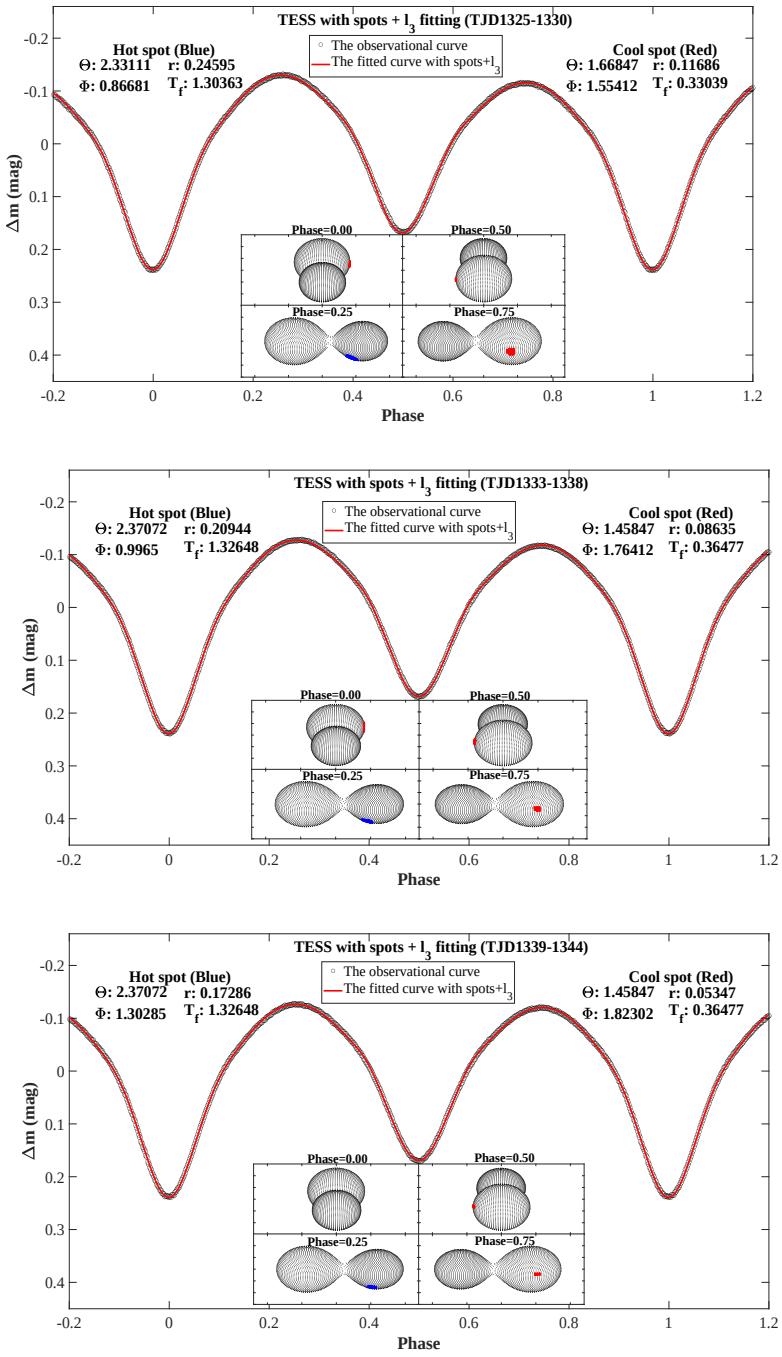

Figure 7. TESS spotted fitting. The three segment TESS asymmetric light curves corresponding to A-B-C (i.e., TJD 1325-1330, TJD 1333-1338, TJD 1339-1344) can be fitted well with an evolving hot spot (blue spot) on the secondary star and an evolving cool spot (red spot) on the primary star. Their positions are roughly symmetrical with the inner Lagrange L1 point. Spot parameters are written in the diagram: the latitude of a star spot center (Θ, in radian), the longitude of a star spot center (Φ, in radian), the radius of a star spot (r, in radian), the temperature factor of a spot (T_f, the ratio of the local spot temperature to the local temperature which would be obtained without the spot).

Table 3. Photometric solutions of BC Gru using the W–D code. The errors are expressed in parenthesis, in units of last decimal places quoted.

Parameter	CASLEO	TESS (TJD1349-1353)	TESS (TJD1325-1330)	TESS (TJD1333-1338)	TESS (TJD1339-1344)	Mean values
	symmetrical LC with l_3	symmetrical LC with l_3	asymmetrical LC spots & l_3	asymmetrical LC spots & l_3	asymmetrical LC spots & l_3	of three spotted solutions
T_1 (K)	5240 (fixed)	5240 (fixed)	5240 (fixed)	5240 (fixed)	5240 (fixed)	5240 (fixed)
$i(^{\circ})$	67.10(12)	70.30(18)	70.31(17)	71.42(16)	71.44(15)	71.06(30)
$q\ (M_2/M_1)$	0.71034(60)	0.68127(89)	0.6904(20)	0.7211(22)	0.7214(23)	0.71(1)
T_2/T_1	0.94046(65)	0.92672(46)	0.92385(41)	0.89905(36)	0.90019(37)	0.9077(66)
$\Omega_1 = \Omega_2$	3.25878(12)	3.17799(16)	3.1914(27)	3.2231(28)	3.2239(29)	3.2128(87)
$L_1/(L_1+L_2)_B$	0.6823(14)	-	-	-	-	-
$L_1/(L_1+L_2)_V$	0.6622(14)	-	-	-	-	-
$L_1/(L_1+L_2)_{R_c}$	0.6473(15)	-	-	-	-	-
$L_1/(L_1+L_2)_{I_c}$	0.6370(16)	-	-	-	-	-
$L_3/(L_1+L_2+L_3)_B$	0.0943(54)	-	-	-	-	-
$L_3/(L_1+L_2+L_3)_V$	0.0010(66)	-	-	-	-	-
$L_3/(L_1+L_2+L_3)_{R_c}$	0.0304(64)	-	-	-	-	-
$L_3/(L_1+L_2+L_3)_{I_c}$	0.0755(61)	-	-	-	-	-
$L_1/(L_1+L_2)_{TESS}$	-	0.6613(20)	0.6615(19)	0.6789(16)	0.6776(16)	0.6727(79)
$L_3/(L_1+L_2+L_3)_{TESS}$	-	0.2104(55)	0.2173(53)	0.2565(40)	0.2566(39)	0.2435(107)
r_1(pole)	0.385229(81)	0.39308(13)	0.39232(19)(42)	0.39179(17)	0.39181(17)	0.39197(14)
r_1(side)	0.40662(11)	0.41605(17)	0.41523(23)	0.41503(20)	0.41505(20)	0.41510(5)
r_1(back)	0.43644(18)	0.44761(29)	0.44700(30)	0.44862(26)	0.44861(26)	0.44808(44)
r_2(pole)	0.32830(12)	0.32931(19)	0.33067(82)(53)	0.33785(85)	0.33754(89)	0.33535(191)
r_2(side)	0.34364(15)	0.34527(24)	0.3468(10)	0.3551(11)	0.3547(11)	0.3522(22)
r_2(back)	0.37576(26)	0.38006(43)	0.3817(17)	0.3920(18)	0.3915(19)	0.3884(27)
f (%)	0.6(3)	8.2(4)	8.8(7)	13.9(7)	13.8(7)	12.2(1.4)
r_1	0.410866(72)	0.42075(12)	0.42012(14)	0.42069(12)	0.42062(12)	0.42048(15)
r_2	0.35069(10)	0.35347(17)	0.35516(68)	0.36346(72)	0.36343(75)	0.36068(225)
R_2/R_1	0.85354(30)	0.84010(47)	0.8454(17)	0.8640(17)	0.8640(18)	0.8578(51)
Mean residual	0.0016	0.00062	0.00057	0.00055	0.00056	...

ple system (Liao et al. 2019, 2021, 2022) and the masses of binary components, the orbital parameters of the third body in BC Gru system were derived and listed in the Table 2. The minimum mass of the third body was estimated to be $M_{3min} = 0.27\,(\pm0.04)$ $M_{\odot}$, and the maximum orbital semi-major axis was $15.43\,(\pm2.74)$ au. The third body is orbiting the central eclipsing binary in an eccentric orbit ($e_3 = 0.17\,(\pm0.08)$). From the FEROS spectrum of BC Gru in Fig. 2 given by Dall et al. (2007), it can be preliminarily inferred that the third component should be a late K-type star. Additionally, photometric solutions of present paper and Moriarty (2016) both suggest the third light contribution in red band is the highest, indicating that the third body should be a late K-type star. If it is a single main-sequence star, it is most likely a K9 type star with less mass (0.59 $M_{\odot}$) than the secondary component of binary. Then the orbital parameters of such tertiary companion would be derived and listed in the lower part of Table 2. The orbital inclination is determined to be $i_3 \sim 30^{\circ}$, which reveals that the third body is non-coplanar to the orbit of the central eclipsing binary. By using the orbital separation of the tertiary $d_3 = a_{12} + a_3 = 19.28$ au, the orbital period of $P_3 = 58.37$ years, the expected mean velocity of the third body can be easily estimated to be 9.84 km s^{-1} ($V_3 = 2\pi d_3/P_3$, assuming the third body moves in an approximately circular orbit around eclipsing pair). Using the parallax value of the Gaia EDR3, the Gaia distance of BC Gru is calculated to be $188.84\,(\pm30.94)$ pc. Thus, the angular separation between the tertiary and the central eclipsing binary is then determined to be $0''.10$.

The present TESS and CASLEO LCs solutions suggested that BC Gru is a spotted evolution A-subtype shallow-contact binary with a mass ratio of 0.71, not a W-subtype derived by previous authors. The third light contribution in red band direction is higher indicates that it is probably a late K-type star. If the third body is a single 0.59 solar mass main-sequence star (K9), based on the relationship of $L \sim M^{3.37}$ (Kippenhahn et al. 2012), it should contribute about 17 % light to the total system. The short-time scale variations in O'Connell effect are discovered during TESS observarions, which could be caused by the evolution of a cool spot on the primary component and a hot spot on the secondary component. It is found that their positions are roughly symmetrical with the inner Lagrange L1 point, which is like that in some analyses (e.g., Shi et al. 2021, Li et al. 2023).

Furthermore, this study reports a discovery of the correlation between the O'Connell effect and the $(O-C)$ curve during TESS observations. The variations of Max I and Max II coincide with the $(O-C)$ curve of the primary and secondary light minima during TESS observations, which indicates that the very low amplitude variability in the $(O-C)$ curve ($\sim$ 0.0006 day) is most likely caused by star spots (Kalimeris et al. 2002; Moriarty 2016). All of our results indicate that BC Gru is an A-subtype shallow-contact binary with spots evolution in a hierarchical triple system.

6 ACKNOWLEDGMENTS

This work is supported by the National Natural Science Foundation of China (No.11933008), the basic research project of Yunnan Province (Grant No. 202201AT070092) and the Natural Science Foundation of Anhui Province (2208085QA23). We acknowledge with sincerest thanks the CASLEO telescope allocation committee and staff members and night assistants of CASLEO for their support.

The TESS data presented in this paper were obtained from the Mikulski Archive for Space Telescopes (MAST) at the Space Telescope Science Institute (STScI). STScI is operated by the Association of Universities for Research in Astronomy, Inc. Support to MAST for these data is provided by the NASA Office of Space Science. Funding for the TESS mission is provided by the NASA Explorer Program.

This work makes use of data from the European Space Agency (ESA) mission Gaia (http-

s://www.cosmos.esa.int/gaia), processed by the Gaia Data Processing and Analysis Consortium (DPAC, https://www.cosmos.esa.int/web/gaia/dpac/consortium). Funding for the DPAC has been provided by national institutions, in particular the institutions participating in the Gaia Multilateral Agreement.

7 DATA AVAILABILITY

The data underlying this article will be shared on reasonable request to the corresponding author.

REFERENCES

Agarwal, A.; Cellone, S. A.; Andruchow, I.; Mammana, L.; Singh, M.; et al., 2019, MNRAS, 488, 4093
Avvakumova, E. A.; Malkov, O. Y.; & Kniazev, A. Y. 2013, AN, 334, 860
Cox, A. N. 2000, Allen's Astrophysical Quantities (New York: AIP)
Dall, T. H.; Foellmi, C.; Pritchard, J.; Lo Curto, G.; Allende Prieto, C.; et al., 2007, A&A, 470, 1202
D'Angelo, C.; van Kerkwijk, M. H.; & Rucinski, S. M. 2006, AJ, 132, 650
Gaia Collaboration 2020, yCat, I/350
Gomez, M.; Lapasset, E.; Ahumada, J.; Clariá, J. J.; & Minniti, D. 1988, BAAA, 34, 119
Hoffmeister, C. 1963, Veroff. Sternwarte Sonnenberg, 6, 1
Irwin, J. B. 1952, ApJ, 116, 211
Juryšek, J.; Hoňková, K.; Šmelcer, L.; Mašek, M.; Lehký, M.; et al., 2017, OEJV, 179, 1
Kalimeris, A.; Rovithis-L. H.; & Rovithis, P. 2002, A&A, 387, 969
Kholopov, P. N.; Kukarkina, N. P.; & Perova, N. B. 1978, IBVS, 1414, 1K
Kholopov, P. N.; Samus, N. N.; Kazarovets, E. V.; & Perova, N. B. 1985, IBVS, 2681, 1
Kippenhahn, R.; Weigert, A.; & Weiss, A. 2012, Stellar Structure and Evolution (2nd ed; Heidelberg: Springer)
Kordopatis, G.; Gilmore, G.; Steinmetz, M.; Boeche, C.; Seabroke, G. M.; et al., 2013, AJ, 146, 134
Kunder, A.; Kordopatis, G.; Steinmetz, M.; Zwitter, T.; McMillan, P. J.; et al., 2017, AJ, 153, 75
Kwee, K. K., & van Woerden, H. 1956, BAN, 12, 327
Latković, O.; Čeki, A.; & Lazarević, S. 2021, ApJS, 254, 10
Li, P.; Liao, W. P.; Qian, S. B.; Li, L. J.; Fang, X. H.; et al. 2023, under review
Liao, W. P.; Qian, S. B.; & Li, L. J. 2021, MNRAS, 508, 6111
Liao, W. P.; Qian, S. B.; & Sarotsakulchai, T. 2019, AJ, 157, 207
Liao, W. -P.; Qian, S. -B.; Shi, X. -D.; Li, L. -J.; Liu, N. -P.; et al., 2022, ApJ, 927, 183
Liu, N. -P.; Qian, S. -B.; Liao, W. -P.; Huang, Y.; & Yuan, Z. -L. 2023, AJ, 165, 259
Meinunger, I. 1979, VeSon, 9, 105
Moriarty, D. J. W. 2016, JAVSO, 44, 10
O'Connell, D. J. K. 1951, PRCO, 2, 85
Paschke, A. 2010, OEJV, 130, 1
Pecaut, M. J.; & Mamajek, E. E. 2013, ApJS, 208, 9
Plewa, T.; & Kałużny, J. 1992, AcA, 42, 103
Pribulla, T.; Kreiner, J. M.; & Tremko, J. 2003, CoSka, 33, 38
Pribulla, T.; & Rucinski, S. M. 2006, AJ, 131, 2986
Ricker, G. R.; Winn, J. N.; Vanderspek, R.; Latham, D. W.; Bakos, G. Á.; et al., 2015, JATIS, 1, 014003
Rucinski, S. M.; Pribulla, T.; & van Kerkwijk, M. H. 2007, AJ, 134, 2353
Samec, R. G.; & Becker, K. 1993, IBVS, 3891, 1
Shank, D.; Komater, D.; Beers, T. C.; Placco, V. M.; & Huang, Y. 2022, ApJS, 261, 19
Shi, X. D.; Qian, S. B.; Li, L. J.; & Liao, W. P. 2021, MNRAS, 505, 6166
Shi, X. D.; Qian, S. B.; Li, L. J.; & Liu, N. P. 2021, AJ, 161, 46
Steinmetz, M.; Guiglion, G.; McMillan, P. J.; Matijevič, G.; Enke, H.; et al., 2020, AJ, 160, 83
Van Hamme, W.; & Wilson, R. E. 2007, ApJ, 661, 1129
Wilson, R. E. 2012, AJ, 144, 73
Wilson, R. E., & Devinney, E. J. 1971, ApJ, 166, 605

Table 1: A total of 399 times of light minima for BC Gru.

Eclipse Times (HJD 2400000+)	Error(±days)	Eclipse(P/S)	Source	Epoch	O-C(days)	Ref.
36814.292		P	Literature	-70089	0.0279	(1)
46686.65316	0.00007	S	Literature	-37963.5	0.0301	(2)
46686.80628	0.00027	P	Literature	-37963	0.0296	(2)
46687.72825	0.00019	P	Literature	-37960	0.0297	(2)
46688.80488	0.00019	S	Literature	-37956.5	0.0307	(2)
46690.64873	0.00032	S	Literature	-37950.5	0.0307	(2)
47375.78278	0.00013	P	Literature	-35721	0.0261	(3)
48473.7799	0.0004	P	Literature	-32148	0.0188	(4)
48474.7021	0.0003	P	Literature	-32145	0.0191	(4)
48478.6964	0.0003	P	Literature	-32132	0.0184	(4)
48479.7726	0.0003	S	Literature	-32128.5	0.0191	(4)
48479.9266		P	Literature	-32128	0.0194	(5)
52134.69500	0.00211	P	Literature	-20235	-0.0024	(6)
52505.92000	0.00211	P	Literature	-19027	-0.0031	(6)
52829.82100	0.00211	P	Literature	-17973	-0.0026	(6)
53367.29600	0.00211	P	Literature	-16224	-0.0058	(6)
53597.46700	0.00211	P	Literature	-15475	-0.0070	(6)
54314.41500	0.00211	P	Literature	-13142	-0.0039	(6)
54632.78100	0.00211	P	Literature	-12106	-0.0069	(6)
55398.58800	0.00300	P	Literature	-9614	-0.0065	(1)
56930.97436	0.00114	S	Literature	-4627.5	-0.0015	(6)
56930.97363	0.00106	S	Literature	-4627.5	-0.0022	(6)
56930.97445	0.00133	S	Literature	-4627.5	-0.0014	(6)
56931.12715	0.00115	P	Literature	-4627	-0.0023	(6)
56931.12722	0.00111	P	Literature	-4627	-0.0023	(6)
56931.12745	0.00121	P	Literature	-4627	-0.0020	(6)
56946.95300	0.00116	S	Literature	-4575.5	-0.0027	(6)
56946.95342	0.00128	S	Literature	-4575.5	-0.0023	(6)
56946.95355	0.00147	S	Literature	-4575.5	-0.0022	(6)
56947.10552	0.00097	P	Literature	-4575	-0.0039	(6)
56947.10617	0.00112	P	Literature	-4575	-0.0032	(6)
56947.10676	0.00112	P	Literature	-4575	-0.0026	(6)
57244.11610	0.00151	S	Literature	-3608.5	-0.0045	(6)
57244.11729	0.00126	S	Literature	-3608.5	-0.0034	(6)
57244.11804	0.00171	S	Literature	-3608.5	-0.0026	(6)
57244.27030	0.00133	P	Literature	-3608	-0.0040	(6)
57244.27043	0.00107	P	Literature	-3608	-0.0039	(6)
57244.27060	0.00143	P	Literature	-3608	-0.0037	(6)
57252.26003	0.00092	P	Literature	-3582	-0.0042	(6)

57252.26021	0.00107	P	Literature	-3582	-0.0040	(6)
57273.92547	0.00133	S	Literature	-3511.5	-0.0039	(6)
57273.92569	0.00136	S	Literature	-3511.5	-0.0036	(6)
57273.92648	0.00144	S	Literature	-3511.5	-0.0029	(6)
57274.07837	0.0009	P	Literature	-3511	-0.0046	(6)
57274.07883	0.00104	P	Literature	-3511	-0.0042	(6)
57274.07904	0.00107	P	Literature	-3511	-0.0039	(6)
57274.23204	0.00136	S	Literature	-3510.5	-0.0046	(6)
57274.23275	0.00133	S	Literature	-3510.5	-0.0039	(6)
57274.23282	0.00134	S	Literature	-3510.5	-0.0038	(6)
57302.04394	0.00113	P	Literature	-3420	-0.0039	(6)
57302.04398	0.00118	P	Literature	-3420	-0.0038	(6)
57599.66995	0.00020	S	Literature	-2451.5	-0.0037	(7)
57602.59040	0.00010	P	Literature	-2442	-0.0027	(7)
58325.37661	0.00009	P	TESS	-90	-0.0002	(8)
58325.53085	0.00012	S	TESS	-89.5	0.0004	(8)
58325.68390	0.00007	P	TESS	-89	-0.0002	(8)
58325.83813	0.00011	S	TESS	-88.5	0.0004	(8)
58325.99121	0.00008	P	TESS	-88	-0.0002	(8)
58326.14537	0.00012	S	TESS	-87.5	0.0003	(8)
58326.29841	0.00009	P	TESS	-87	-0.0003	(8)
58326.45274	0.00011	S	TESS	-86.5	0.0004	(8)
58326.60581	0.00008	P	TESS	-86	-0.0002	(8)
58326.75995	0.00011	S	TESS	-85.5	0.0003	(8)
58326.91313	0.00007	P	TESS	-85	-0.0002	(8)
58327.06724	0.00011	S	TESS	-84.5	0.0002	(8)
58327.22045	0.00007	P	TESS	-84	-0.0002	(8)
58327.37465	0.00011	S	TESS	-83.5	0.0004	(8)
58327.52781	0.00008	P	TESS	-83	-0.0001	(8)
58327.68195	0.00012	S	TESS	-82.5	0.0003	(8)
58327.83516	0.00012	P	TESS	-82	-0.0001	(8)
58327.98926	0.00010	S	TESS	-81.5	0.0003	(8)
58328.14233	0.00007	P	TESS	-81	-0.0002	(8)
58328.29660	0.00012	S	TESS	-80.5	0.0004	(8)
58328.44970	0.00007	P	TESS	-80	-0.0002	(8)
58328.60402	0.00009	S	TESS	-79.5	0.0005	(8)
58328.75704	0.00009	P	TESS	-79	-0.0001	(8)
58328.91128	0.00010	S	TESS	-78.5	0.0005	(8)
58329.06427	0.00008	P	TESS	-78	-0.0002	(8)
58329.21841	0.00011	S	TESS	-77.5	0.0003	(8)
58329.37157	0.00009	P	TESS	-77	-0.0002	(8)
58329.52579	0.00010	S	TESS	-76.5	0.0003	(8)
58329.67895	0.00006	P	TESS	-76	-0.0001	(8)
58329.83321	0.00010	S	TESS	-75.5	0.0005	(8)

58329.98623	0.00009	P	TESS	-75	-0.0002	(8)
58330.14047	0.00010	S	TESS	-74.5	0.0004	(8)
58330.29347	0.00008	P	TESS	-74	-0.0002	(8)
58330.44784	0.00012	S	TESS	-73.5	0.0005	(8)
58330.60080	0.00009	P	TESS	-73	-0.0002	(8)
58330.75505	0.00011	S	TESS	-72.5	0.0004	(8)
58330.90817	0.00008	P	TESS	-72	-0.0001	(8)
58331.06248	0.00009	S	TESS	-71.5	0.0005	(8)
58331.21543	0.00008	P	TESS	-71	-0.0002	(8)
58331.36977	0.00009	S	TESS	-70.5	0.0005	(8)
58331.52264	0.00008	P	TESS	-70	-0.0003	(8)
58331.67716	0.00011	S	TESS	-69.5	0.0006	(8)
58331.98431	0.00010	S	TESS	-68.5	0.0004	(8)
58331.82996	0.00008	P	TESS	-69	-0.0003	(8)
58332.13730	0.00007	P	TESS	-68	-0.0002	(8)
58332.29170	0.00011	S	TESS	-67.5	0.0005	(8)
58332.44464	0.00007	P	TESS	-67	-0.0002	(8)
58332.59894	0.00013	S	TESS	-66.5	0.0004	(8)
58332.75193	0.00008	P	TESS	-66	-0.0002	(8)
58332.90622	0.00011	S	TESS	-65.5	0.0004	(8)
58333.05934	0.00008	P	TESS	-65	-0.0001	(8)
58333.21353	0.00011	S	TESS	-64.5	0.0004	(8)
58333.36663	0.00009	P	TESS	-64	-0.0001	(8)
58333.52077	0.00011	S	TESS	-63.5	0.0004	(8)
58333.67396	0.00008	P	TESS	-63	-0.0001	(8)
58333.82823	0.00009	S	TESS	-62.5	0.0005	(8)
58333.98122	0.00007	P	TESS	-62	-0.0002	(8)
58334.13546	0.00011	S	TESS	-61.5	0.0004	(8)
58334.28861	0.00007	P	TESS	-61	-0.0001	(8)
58334.44269	0.00010	S	TESS	-60.5	0.0004	(8)
58334.59587	0.00008	P	TESS	-60	-0.0001	(8)
58334.74998	0.00010	S	TESS	-59.5	0.0003	(8)
58334.90318	0.00008	P	TESS	-59	-0.0001	(8)
58335.05721	0.00011	S	TESS	-58.5	0.0003	(8)
58335.21045	0.00007	P	TESS	-58	-0.0002	(8)
58335.36462	0.00010	S	TESS	-57.5	0.0004	(8)
58335.51777	0.00009	P	TESS	-57	-0.0001	(8)
58335.67187	0.00010	S	TESS	-56.5	0.0003	(8)
58335.82508	0.00007	P	TESS	-56	-0.0001	(8)
58335.97910	0.00010	S	TESS	-55.5	0.0002	(8)
58336.13238	0.00008	P	TESS	-55	-0.0001	(8)
58336.28640	0.00010	S	TESS	-54.5	0.0002	(8)
58336.43968	0.00008	P	TESS	-54	-0.0001	(8)
58336.59370	0.00009	S	TESS	-53.5	0.0002	(8)

58336.74690	0.00011	P	TESS	-53	-0.0002	(8)
58336.90100	0.00009	S	TESS	-52.5	0.0002	(8)
58337.05435	0.00009	P	TESS	-52	-0.0001	(8)
58337.20833	0.00010	S	TESS	-51.5	0.0002	(8)
58337.36163	0.00009	P	TESS	-51	-0.0001	(8)
58337.51544	0.00009	S	TESS	-50.5	0.0000	(8)
58337.66886	0.00009	P	TESS	-50	-0.0002	(8)
58337.82288	0.00012	S	TESS	-49.5	0.0002	(8)
58337.97629	0.00007	P	TESS	-49	-0.0001	(8)
58338.13021	0.00010	S	TESS	-48.5	0.0002	(8)
58338.28356	0.00008	P	TESS	-48	-0.0001	(8)
58338.43755	0.00009	S	TESS	-47.5	0.0002	(8)
58339.66646	0.00010	S	TESS	-43.5	-0.0001	(8)
58339.82004	0.00009	P	TESS	-43	-0.0002	(8)
58339.97397	0.00010	S	TESS	-42.5	0.0001	(8)
58340.12734	0.00007	P	TESS	-42	-0.0002	(8)
58340.28129	0.00011	S	TESS	-41.5	0.0001	(8)
58340.43467	0.00006	P	TESS	-41	-0.0001	(8)
58340.58863	0.00012	S	TESS	-40.5	0.0002	(8)
58340.74196	0.00006	P	TESS	-40	-0.0002	(8)
58340.89589	0.00012	S	TESS	-39.5	0.0001	(8)
58341.04927	0.00009	P	TESS	-39	-0.0001	(8)
58341.20323	0.00011	S	TESS	-38.5	0.0002	(8)
58341.35649	0.00007	P	TESS	-38	-0.0002	(8)
58341.51039	0.00011	S	TESS	-37.5	0.0000	(8)
58341.66383	0.00007	P	TESS	-37	-0.0002	(8)
58341.81767	0.00011	S	TESS	-36.5	0.0000	(8)
58341.97114	0.00008	P	TESS	-36	-0.0002	(8)
58342.12492	0.00009	S	TESS	-35.5	-0.0001	(8)
58342.27851	0.00009	P	TESS	-35	-0.0001	(8)
58342.43231	0.00011	S	TESS	-34.5	0.0000	(8)
58342.58576	0.00008	P	TESS	-34	-0.0002	(8)
58342.73953	0.00011	S	TESS	-33.5	-0.0001	(8)
58342.89311	0.00009	P	TESS	-33	-0.0001	(8)
58343.04694	0.00011	S	TESS	-32.5	0.0000	(8)
58343.20040	0.00007	P	TESS	-32	-0.0002	(8)
58343.35416	0.00010	S	TESS	-31.5	-0.0001	(8)
58343.50770	0.00009	P	TESS	-31	-0.0002	(8)
58343.66152	0.00011	S	TESS	-30.5	0.0000	(8)
58343.81513	0.00008	P	TESS	-30	0.0000	(8)
58343.96888	0.00012	S	TESS	-29.5	0.0001	(8)
58344.12244	0.00009	P	TESS	-29	0.0000	(8)
58344.27570	0.00050	S	TESS	-28.5	-0.0004	(8)
58344.42961	0.00007	P	TESS	-28	-0.0002	(8)

58344.58339	0.00011	S	TESS	-27.5	0.0000	(8)
58344.73698	0.00009	P	TESS	-27	-0.0001	(8)
58344.89070	0.00014	S	TESS	-26.5	0.0000	(8)
58345.04428	0.00008	P	TESS	-26	-0.0001	(8)
58345.19806	0.00010	S	TESS	-25.5	0.0000	(8)
58345.35157	0.00008	P	TESS	-25	-0.0001	(8)
58345.50539	0.00010	S	TESS	-24.5	0.0000	(8)
58345.65891	0.00010	P	TESS	-24	-0.0001	(8)
58345.81272	0.00011	S	TESS	-23.5	0.0001	(8)
58345.96621	0.00008	P	TESS	-23	-0.0001	(8)
58346.12009	0.00011	S	TESS	-22.5	0.0001	(8)
58346.27354	0.00010	P	TESS	-22	-0.0001	(8)
58346.42734	0.00010	S	TESS	-21.5	0.0001	(8)
58346.58081	0.00007	P	TESS	-21	-0.0001	(8)
58346.73459	0.00013	S	TESS	-20.5	0.0000	(8)
58346.88811	0.00008	P	TESS	-20	-0.0001	(8)
58346.88813	0.00003	P	CASLEO 2.15m	-20	-0.0001	(8)
58347.04186	0.00011	S	TESS	-19.5	0.0000	(8)
58347.19530	0.00009	P	TESS	-19	-0.0002	(8)
58347.35037	0.00070	S	TESS	-18.5	0.0012	(8)
58347.50263	0.00008	P	TESS	-18	-0.0002	(8)
58347.65652	0.00013	S	TESS	-17.5	0.0000	(8)
58347.80965	0.00014	P	TESS	-17	-0.0005	(8)
58347.96382	0.00011	S	TESS	-16.5	0.0000	(8)
58348.11669	0.00011	P	TESS	-16	-0.0008	(8)
58348.42485	0.00009	P	TESS	-15	0.0001	(8)
58348.57872	0.00013	S	TESS	-14.5	0.0003	(8)
58348.73137	0.00015	P	TESS	-14	-0.0007	(8)
58348.88650	0.00037	S	TESS	-13.5	0.0008	(8)
58349.03916	0.00010	P	TESS	-13	-0.0002	(8)
58349.34658	0.00009	P	TESS	-12	-0.0001	(8)
58349.50030	0.00015	S	TESS	-11.5	0.0000	(8)
58349.65398	0.00009	P	TESS	-11	0.0000	(8)
58349.80762	0.00011	S	TESS	-10.5	0.0000	(8)
58349.96124	0.00007	P	TESS	-10	-0.0001	(8)
58350.11491	0.00010	S	TESS	-9.5	0.0000	(8)
58350.26845	0.00007	P	TESS	-9	-0.0001	(8)
58350.42213	0.00009	S	TESS	-8.5	-0.0001	(8)
58350.57581	0.00007	P	TESS	-8	-0.0001	(8)
58350.72951	0.00010	S	TESS	-7.5	0.0000	(8)
58350.88319	0.00008	P	TESS	-7	0.0000	(8)
58351.03696	0.00010	S	TESS	-6.5	0.0001	(8)
58351.19039	0.00008	P	TESS	-6	-0.0001	(8)
58351.34422	0.00010	S	TESS	-5.5	0.0001	(8)

58351.49771	0.00007	P	TESS	-5	-0.0001	(8)
58351.65151	0.00013	S	TESS	-4.5	0.0000	(8)
58351.80507	0.00009	P	TESS	-4	-0.0001	(8)
58351.95875	0.00012	S	TESS	-3.5	0.0000	(8)
58352.11238	0.00009	P	TESS	-3	-0.0001	(8)
58352.26620	0.00010	S	TESS	-2.5	0.0001	(8)
58352.41971	0.00007	P	TESS	-2	0.0000	(8)
58352.57350	0.00011	S	TESS	-1.5	0.0001	(8)
58352.72707	0.00007	P	TESS	-1	0.0000	(8)
58352.88076	0.00010	S	TESS	-0.5	0.0001	(8)
58353.03435	0.00009	P	TESS	0	0.0000	(8)
58365.78787	0.00007	S	CASLEO 0.6m	41.5	0.0003	(8)
58367.63189	0.00010	S	CASLEO 0.6m	47.5	0.0005	(8)
58367.78495	0.00008	P	CASLEO 0.6m	48	-0.0001	(8)
58368.55314	0.00015	S	CASLEO 0.6m	50.5	-0.0002	(8)
58368.70674	0.00008	P	CASLEO 0.6m	51	-0.0002	(8)
58368.86090	0.00021	S	CASLEO 0.6m	51.5	0.0003	(8)
58369.62887	0.00008	P	CASLEO 0.6m	54	0.0000	(8)
58369.78319	0.00014	S	CASLEO 0.6m	54.5	0.0007	(8)
58373.62315	0.00045	P	CASLEO 0.6m	67	-0.0007	(8)
58373.77863	0.00020	S	CASLEO 0.6m	67.5	0.0011	(8)
58375.62187	0.00009	S	CASLEO 0.6m	73.5	0.0005	(8)
58376.54342	0.00008	S	CASLEO 0.6m	76.5	0.0002	(8)
58376.69716	0.00005	P	CASLEO 0.6m	77	0.0002	(8)
58638.82994	0.00007	P	CASLEO 0.6m	930	0.0010	(8)
58642.82426	0.00007	P	CASLEO 0.6m	943	0.0004	(8)
59061.99074	0.00080	P	TESS	2307	0.0014	(8)
59062.14487	0.00052	S	TESS	2307.5	0.0019	(8)
59062.29768	0.00062	P	TESS	2308	0.0011	(8)
59062.45213	0.00055	S	TESS	2308.5	0.0019	(8)
59062.60478	0.00069	P	TESS	2309	0.0009	(8)
59062.75929	0.00038	S	TESS	2309.5	0.0017	(8)
59062.91266	0.00078	P	TESS	2310	0.0014	(8)
59063.06639	0.00045	S	TESS	2310.5	0.0015	(8)
59063.22001	0.00077	P	TESS	2311	0.0015	(8)
59063.37402	0.00058	S	TESS	2311.5	0.0019	(8)
59063.52695	0.00060	P	TESS	2312	0.0011	(8)
59063.68142	0.00054	S	TESS	2312.5	0.0019	(8)
59063.83400	0.00069	P	TESS	2313	0.0009	(8)
59063.98849	0.00043	S	TESS	2313.5	0.0017	(8)
59064.14190	0.00079	P	TESS	2314	0.0015	(8)
59064.29557	0.00043	S	TESS	2314.5	0.0015	(8)
59064.44922	0.00075	P	TESS	2315	0.0015	(8)
59064.60329	0.00058	S	TESS	2315.5	0.0019	(8)

59064.75620	0.00063	P	TESS	2316	0.0012	(8)
59064.91056	0.00053	S	TESS	2316.5	0.0019	(8)
59065.06329	0.00068	P	TESS	2317	0.0009	(8)
59065.21766	0.00040	S	TESS	2317.5	0.0017	(8)
59065.37121	0.00079	P	TESS	2318	0.0016	(8)
59065.52480	0.00047	S	TESS	2318.5	0.0015	(8)
59065.67851	0.00078	P	TESS	2319	0.0015	(8)
59065.83247	0.00059	S	TESS	2319.5	0.0019	(8)
59065.98545	0.00062	P	TESS	2320	0.0012	(8)
59066.13987	0.00055	S	TESS	2320.5	0.0019	(8)
59066.29241	0.00070	P	TESS	2321	0.0008	(8)
59066.44690	0.00038	S	TESS	2321.5	0.0017	(8)
59066.60038	0.00078	P	TESS	2322	0.0015	(8)
59066.75401	0.00047	S	TESS	2322.5	0.0015	(8)
59066.90763	0.00078	P	TESS	2323	0.0014	(8)
59067.06175	0.00053	S	TESS	2323.5	0.0019	(8)
59067.21456	0.00063	P	TESS	2324	0.0011	(8)
59067.36914	0.00058	S	TESS	2324.5	0.0020	(8)
59067.52165	0.00069	P	TESS	2325	0.0009	(8)
59067.67611	0.00040	S	TESS	2325.5	0.0017	(8)
59067.82948	0.00080	P	TESS	2326	0.0014	(8)
59067.98365	0.00058	S	TESS	2326.5	0.0019	(8)
59068.13687	0.00076	P	TESS	2327	0.0015	(8)
59068.29093	0.00057	S	TESS	2327.5	0.0019	(8)
59068.44384	0.00066	P	TESS	2328	0.0011	(8)
59068.59831	0.00053	S	TESS	2328.5	0.0019	(8)
59068.75095	0.00069	P	TESS	2329	0.0009	(8)
59068.90536	0.00038	S	TESS	2329.5	0.0017	(8)
59069.05882	0.00077	P	TESS	2330	0.0015	(8)
59069.21248	0.00044	S	TESS	2330.5	0.0015	(8)
59069.36613	0.00075	P	TESS	2331	0.0015	(8)
59069.52028	0.00054	S	TESS	2331.5	0.0020	(8)
59069.67305	0.00062	P	TESS	2332	0.0011	(8)
59069.82758	0.00052	S	TESS	2332.5	0.0020	(8)
59069.98015	0.00071	P	TESS	2333	0.0009	(8)
59070.13463	0.00038	S	TESS	2333.5	0.0017	(8)
59070.28811	0.00080	P	TESS	2334	0.0016	(8)
59070.44178	0.00046	S	TESS	2334.5	0.0016	(8)
59070.59539	0.00078	P	TESS	2335	0.0015	(8)
59070.74955	0.00055	S	TESS	2335.5	0.0020	(8)
59070.90235	0.00060	P	TESS	2336	0.0012	(8)
59071.05689	0.00054	S	TESS	2336.5	0.0021	(8)
59071.20941	0.00071	P	TESS	2337	0.0009	(8)
59071.36390	0.00041	S	TESS	2337.5	0.0018	(8)

59071.51728	0.00077	P	TESS	2338	0.0015	(8)
59071.67105	0.00048	S	TESS	2338.5	0.0016	(8)
59071.82461	0.00078	P	TESS	2339	0.0015	(8)
59071.97884	0.00056	S	TESS	2339.5	0.0021	(8)
59072.13151	0.00061	P	TESS	2340	0.0011	(8)
59072.28624	0.00054	S	TESS	2340.5	0.0022	(8)
59072.43855	0.00070	P	TESS	2341	0.0009	(8)
59072.59330	0.00040	S	TESS	2341.5	0.0020	(8)
59072.74643	0.00079	P	TESS	2342	0.0014	(8)
59072.90039	0.00043	S	TESS	2342.5	0.0017	(8)
59073.05380	0.00080	P	TESS	2343	0.0015	(8)
59073.20816	0.00055	S	TESS	2343.5	0.0022	(8)
59073.36067	0.00065	P	TESS	2344	0.0011	(8)
59073.51559	0.00052	S	TESS	2344.5	0.0023	(8)
59073.66779	0.00069	P	TESS	2345	0.0009	(8)
59073.82250	0.00041	S	TESS	2345.5	0.0019	(8)
59075.20495	0.00081	P	TESS	2350	0.0015	(8)
59075.35894	0.00047	S	TESS	2350.5	0.0018	(8)
59075.51202	0.00062	P	TESS	2351	0.0013	(8)
59075.66671	0.00053	S	TESS	2351.5	0.0023	(8)
59075.81917	0.00063	P	TESS	2352	0.0011	(8)
59075.97403	0.00047	S	TESS	2352.5	0.0023	(8)
59076.12623	0.00073	P	TESS	2353	0.0009	(8)
59076.28107	0.00038	S	TESS	2353.5	0.0020	(8)
59076.43427	0.00077	P	TESS	2354	0.0016	(8)
59076.58817	0.00049	S	TESS	2354.5	0.0018	(8)
59076.74152	0.00076	P	TESS	2355	0.0015	(8)
59076.89596	0.00052	S	TESS	2355.5	0.0023	(8)
59077.04849	0.00065	P	TESS	2356	0.0012	(8)
59077.20336	0.00048	S	TESS	2356.5	0.0024	(8)
59077.35552	0.00073	P	TESS	2357	0.0009	(8)
59077.51030	0.00040	S	TESS	2357.5	0.0021	(8)
59077.66354	0.00080	P	TESS	2358	0.0016	(8)
59077.81727	0.00047	S	TESS	2358.5	0.0017	(8)
59077.97062	0.00062	P	TESS	2359	0.0014	(8)
59078.12506	0.00051	S	TESS	2359.5	0.0022	(8)
59078.27771	0.00064	P	TESS	2360	0.0012	(8)
59078.43243	0.00052	S	TESS	2360.5	0.0023	(8)
59078.58476	0.00073	P	TESS	2361	0.0009	(8)
59078.73943	0.00042	S	TESS	2361.5	0.0020	(8)
59078.89278	0.00078	P	TESS	2362	0.0017	(8)
59079.04654	0.00050	S	TESS	2362.5	0.0018	(8)
59079.19987	0.00061	P	TESS	2363	0.0014	(8)
59079.35432	0.00053	S	TESS	2363.5	0.0022	(8)

59079.50696	0.00063	P	TESS	2364	0.0012	(8)
59079.66159	0.00055	S	TESS	2364.5	0.0022	(8)
59079.81398	0.00073	P	TESS	2365	0.0009	(8)
59079.96861	0.00043	S	TESS	2365.5	0.0019	(8)
59080.12201	0.00080	P	TESS	2366	0.0017	(8)
59080.27579	0.00050	S	TESS	2366.5	0.0018	(8)
59080.42909	0.00062	P	TESS	2367	0.0014	(8)
59080.58354	0.00049	S	TESS	2367.5	0.0022	(8)
59080.73616	0.00065	P	TESS	2368	0.0012	(8)
59080.89085	0.00056	S	TESS	2368.5	0.0022	(8)
59081.04319	0.00074	P	TESS	2369	0.0009	(8)
59081.19769	0.00036	S	TESS	2369.5	0.0018	(8)
59081.35118	0.00082	P	TESS	2370	0.0016	(8)
59081.50495	0.00050	S	TESS	2370.5	0.0017	(8)
59081.65827	0.00062	P	TESS	2371	0.0014	(8)
59081.81274	0.00050	S	TESS	2371.5	0.0022	(8)
59081.96542	0.00065	P	TESS	2372	0.0012	(8)
59082.12007	0.00049	S	TESS	2372.5	0.0022	(8)
59082.27242	0.00073	P	TESS	2373	0.0009	(8)
59082.42697	0.00039	S	TESS	2373.5	0.0018	(8)
59082.58049	0.00080	P	TESS	2374	0.0017	(8)
59082.73414	0.00046	S	TESS	2374.5	0.0017	(8)
59082.88752	0.00060	P	TESS	2375	0.0014	(8)
59083.04195	0.00048	S	TESS	2375.5	0.0022	(8)
59083.19464	0.00067	P	TESS	2376	0.0012	(8)
59083.34929	0.00051	S	TESS	2376.5	0.0022	(8)
59083.50177	0.00074	P	TESS	2377	0.0011	(8)
59083.65626	0.00040	S	TESS	2377.5	0.0019	(8)
59083.80981	0.00081	P	TESS	2378	0.0018	(8)
59083.96338	0.00049	S	TESS	2378.5	0.0017	(8)
59084.11683	0.00065	P	TESS	2379	0.0015	(8)
59084.27125	0.00054	S	TESS	2379.5	0.0023	(8)
59084.42398	0.00066	P	TESS	2380	0.0013	(8)
59084.57859	0.00054	S	TESS	2380.5	0.0023	(8)
59084.73103	0.00075	P	TESS	2381	0.0011	(8)
59084.88549	0.00046	S	TESS	2381.5	0.0019	(8)
59085.03912	0.00078	P	TESS	2382	0.0019	(8)
59085.19255	0.00050	S	TESS	2382.5	0.0017	(8)
59085.34612	0.00062	P	TESS	2383	0.0016	(8)
59085.50050	0.00051	S	TESS	2383.5	0.0023	(8)
59085.65319	0.00066	P	TESS	2384	0.0013	(8)
59085.80779	0.00052	S	TESS	2384.5	0.0023	(8)
59085.96023	0.00077	P	TESS	2385	0.0011	(8)
59086.11482	0.00043	S	TESS	2385.5	0.0020	(8)

59086.26837	0.00084	P	TESS	2386	0.0019	(8)
59086.42194	0.00049	S	TESS	2386.5	0.0018	(8)
59086.57526	0.00062	P	TESS	2387	0.0015	(8)
59086.72977	0.00055	S	TESS	2387.5	0.0023	(8)
59086.88274	0.00083	P	TESS	2388	0.0017	(8)
59491.60682	0.00007	P	CASLEO 0.6m	3705	0.0037	(8)
59813.66589	0.00006	P	CASLEO 0.6m	4753	0.0061	(8)
60206.71151	0.00012	P	CASLEO 0.6m	6032	0.0074	(8)

References: (1)Paschke, A. (2010); (2) Plewa & Kaluzny (1992); (3) Gomez et al. (1988); (4) Samec & Becker (1993); (5) Pribulla et al. (2003); (6) Moriarty (2016); (7) Jurysek et al. (2017); (8) This paper.